Effect of annealing on the segregation in $(Fe_{64}Mn_{36})_{35}Y_{65}$ metallic glass

1992 J. Phys.: Condens. Matter 4 1241

(http://iopscience.iop.org/0953-8984/4/5/004)

J. Phys.: Condens. Matter 4 (1992) 1241–1250. Printed in the UK

Effect of annealing on the segregation in $(Fe_{64}Mn_{36})_{35}Y_{65}$ metallic glass

M Maret†, J P Simon† and O Lyon‡

† Laboratoire de Thermodynamique et Physico-Chimie Métallurgiques, Unité de Recherche associée au CNRS 29, Institut National Polytechnique de Grenoble, Ecole Nationale Supérieure d'Electrochimie et d'Electrométallurgie de Grenoble, BP 75, 38402 Saint Martin d'Hères Cédex, France

‡ Laboratoire d'Utilisation du Rayonnement Electromagnétique, Bâtiment 209 D, 91405 Orsay Cédex, France

Received 26 July 1991

Abstract. The effect of annealing on the segregation in $(Fe_{64}Mn_{36})_{35}Y_{65}$ metallic glass has been studied by anomalous small-angle x-ray scattering in conjunction with conventional x-ray scattering and differential scanning calorimetry measurements. From the Ornstein–Zernike theory, it has been found that the structural relaxation takes place through an increase in the concentration fluctuations (already present in the as-quenched ribbons) and a small decrease of their correlation length. The crystallization of HCP Y is never preceded by an amorphous phase separation but occurs by nucleation-and-growth processes. It is then a classical primary crystallization. From the anomalous dispersion technique the ratio of the atomic volumes in the amorphous alloy does not change significantly during the crystallization of Y.

1. Introduction

Recently, we have shown that, in the as-quenched state, the segregating $(Fe_xMn_{1-x})_{35}Y_{65}$ metallic glasses develop a medium-range order (on a scale of about 10 Å) revealed by small-angle x-ray scattering (SAXS), while the chemically ordered $Ni_{33}Y_{67}$ glass and the disordered $Cu_{33}Y_{67}$ glass exhibit no such order (Maret *et al* 1989). From the Ornstein–Zernike (OZ) theory this medium-range order has been described in terms of concentration fluctuations, yielding a segregation between transition metal (M) and yttrium atoms (the absence of an interference halo in our SAXS data excludes phase separation into two amorphous phases). Moreover, it has been demonstrated that as in two-phase binary systems the SAXS intensity stemming from concentration and density fluctuations is proportional to the square of the difference of the atomic scattering factor densities of the two species: $(f_M/V_M - f_Y/V_Y)(f_M/V_M - f_Y/V_Y)^*$ with M ≡ Mn or Fe (f_i is the complex scattering factor given by $f_i = Z_i + f_i'(E) + f_i''(E)$). The anomalous SAXS technique applied below the Mn absorption edge has allowed us to determine the ratio V_M/V_Y of the partial atomic volumes in these pseudo-binary glasses. It was found to be very close to the ratio of the atomic volumes of pure metals.

In the present paper, we analyse the effect of annealing up to the onset of the primary crystallization of the HCP Y phase on the segregating medium-range order in the

0953-8984/92/051241 + 10 $04.50

$(Fe_{64}Mn_{36})_{35}Y_{65}$ metallic glass by SAXS in conjunction with conventional x-ray diffraction (XRD) and differential scanning calorimetry (DSC) measurements. Preliminary SAXS measurements on $(Fe_{64}Mn_{36})_{35}Y_{65}$ ribbons annealed at 513 K for 1 h (the onset temperature of HCP Y crystallization measured by DSC with a heating rate of 40 K min^{-1} being 600 K) have shown an increase in concentration fluctuations $S_{CC}(0)$ together with a small decrease in their correlation length ξ. This result contrasts with the simultaneous increase in $S_{CC}(0)$ and ξ observed in binary crystalline or liquid alloys when approaching a miscibility gap. The aim of this new series of SAXS experiments will be to follow the change in ξ after annealing at temperatures still closer to the crystallization temperature. That should allow us to know whether the crystallization reaction is preceded with phase separation into a transition-metal-enriched amorphous phase and Y particles playing the role of pre-existing nuclei.

2. Experimental technique

Amorphous ribbons (1 mm wide and 20 μm thick) of $(Fe_{64}Mn_{36})_{35}Y_{65}$ alloys were produced by the melt-spinning technique. Ribbons were annealed in sealed evacuated Pyrex tubes. Two series of annealing treatments were performed: one series at the same temperature of 533 K with annealing times t_a varying from 10 min to 4 d and a second series at temperatures ranging from 553 to 573 K for t_a = 30 min. The SAXS experiments were performed on beam line D22 of the synchrotron radiation facility of Laboratoire d'Utilisation du Rayonnement Electromagnétique (Orsay) using a double Ge[111] monochromator and a linear position-sensitive detector. The anomalous SAXS measurements were carried out at x-ray energies from 6260 to 6531 eV below the Mn absorption edge (6539 eV). Using a sample–detector distance of 216 mm, the scattering intensity was measured over a q-range from 4×10^{-2} to 0.55 $Å^{-1}$. The x-ray samples constituted by a unique piece of ribbon were centred in the beam 0.25 mm high and 3 mm wide by measuring their transmission. The intensities were corrected for background, sample absorption and detector efficiencies in position and in energy and finally normalized from the Fe fluorescence (Simon and Lyon 1989). The q-independent contributions of the sample fluorescence and resonant Raman scattering were subtracted by assuming an asymptotic behaviour of the sample scattering in q^{-2} beyond 0.4 $Å^{-1}$. X-ray diffraction patterns of annealed ribbons (using Cu Kα radiation) were recorded in reflection geometry such that the surface of ribbon in contact with the wheel was exposed. The thermal analysis experiments were carried out in a Perkin–Elmer DSC-II differential scanning calorimeter under an At atmosphere using specimens of mass from 5 to 8 mg.

3. Results

Figures 1 and 2 show the change in the SAXS intensity for ribbons of $(Fe_{64}Mn_{36})_{35}Y_{65}$ with annealing treatment (the curves are the averages obtained below the Mn edge). In figure 1, for short annealing times ($t_a \leq$ 1 h), the intensity of ribbons annealed at 533 K increases over the whole q-range. For longer times, we can distinguish two regions: above 0.25 $Å^{-1}$, the change in $I(Q)$ becomes very small and, below 0.25 $Å^{-1}$, $I(q)$ increases gradually with increasing annealing time and then strongly after a treatment of 24 h. Figure 2 displays the change in $I(q)$ after higher-temperature annealing treatments for 30 min. The effects of annealing treatments at 553 K and 573 K for 30 min are quite

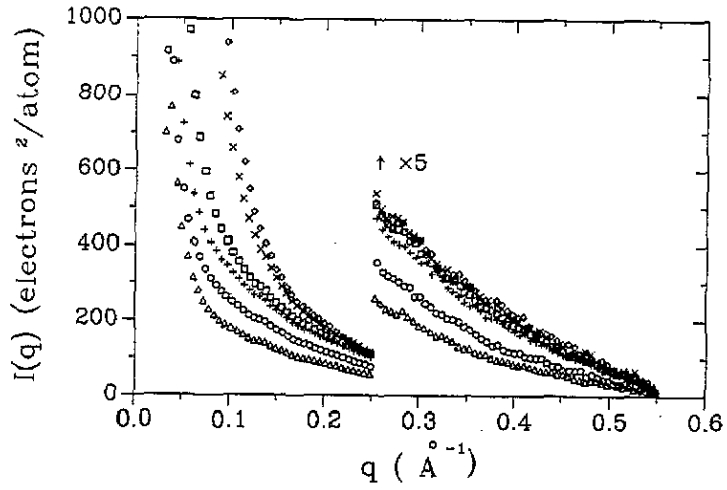

Figure 1. Change in the SAXS intensity with annealing time at 533 K for $(Fe_{64}Mn_{36})_{35}Y_{65}$ metallic glass using as-quenched samples (△) and samples annealed at 533 K for 10 min (○), 1 h (+), 6 h (□), 24 h (×) and 4 d (◇).

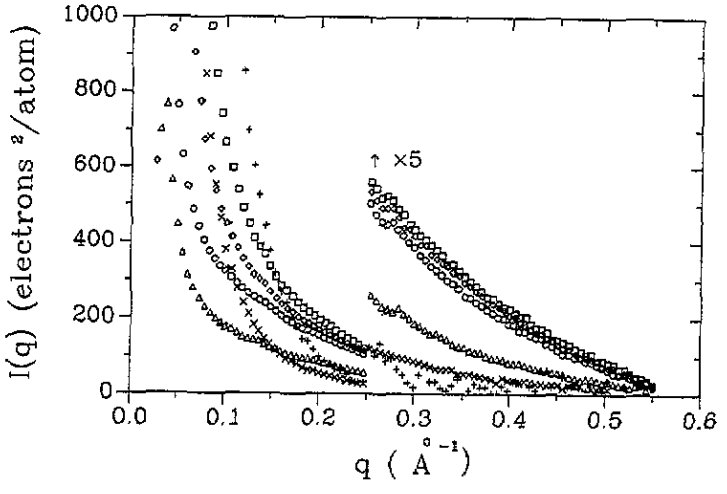

Figure 2. SAXS intensities of $(Fe_{64}Mn_{36})_{35}Y_{65}$ ribbons using as-quenched samples (△), samples annealed for 30 min at 553 K (○), 563 K (◇) and 573 K (□), samples partially crystallized after an anneal at 700 K for 1 h (+) and samples fully crystallized after an anneal at 873 K for 1 h (×).

comparable with those obtained at 533 K for 1 h and 24 h, respectively. Again, above 0.25 $Å^{-1}$, the level of the SAXS intensity is attained after an anneal at 553 K while, below 0.25 $Å^{-1}$, $I(q)$ increases continuously with increasing annealing temperature. For comparison, we have also drawn in figure 2 the intensities scattered by ribbons after treatments at temperatures of 700 K and 873 K which correspond to the ends of the two crystallization steps, the first yielding the formation of the HCP Y phase and an Fe-enriched amorphous phase and the second the formation of the Laves phase $(Fe–Mn)_2Y$

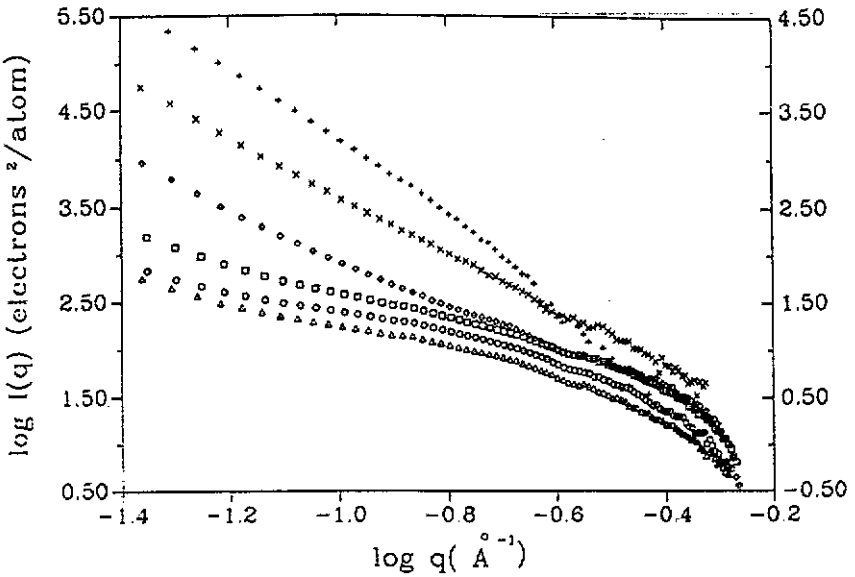

Figure 3. A log–log representation of the SAXS curves selected in figures 1 and 2 and corresponding to $(Fe_{64}Mn_{36})_{35}Y_{65}$ ribbons using as-quenched samples (△), samples annealed at 533 K for 10 min (○), 6 h (□) and 4 d (◇), samples annealed at 700 K for 1 h (+) and samples annealed at 873 K for 1 h (×). (To emphasize the linear behaviour, the last two curves (+, ×) are shifted towards the top of the figure and refer to the right-hand scale.)

and the growth of HCP Y. The intensities of partially and fully crystallized ribbons show a strong increase at smaller q-values more especially after the anneal at 873 K and become negligible above 0.3 $Å^{-1}$.

A log–log representation of the scattering intensities of ribbons in different states (as quenched, annealed and crystallized) is displayed in figure 3. For as-quenched ribbons and those annealed at 533 K for less than 1 d a continuously curved behaviour is observed, while for an annealing time of 4 d, the low-q part becomes straight. For ribbons annealed at 700 and 873 K a linear variation is observed over almost the whole q-range. The exponent of the scattering law in q^{-n} depends on the state of the ribbon; n is equal to 3.8 for ribbons containing Y crystallites and an Fe-enriched amorphous phase and to 3 for ribbons that are fully crystallized.

The change in x-ray patterns of ribbons annealed at 533 K with increasing annealing time is shown in figure 4 together with the patterns of partially and fully crystallized ribbons. The small Bragg peaks visible in the pattern of the as-quenched sample are assigned to crystals of hexagonal Y_2O_3 distributed preferentially on the ribbon surface. For annealing times $t_a \leq 3$ h a small peak at $2\theta = 32.3°$ is superimposed on the first peak of the structure factor of the amorphous alloy; it can be indexed as the 101 reflection of HCP Y. For still longer times, this peak becomes sharper and other peaks corresponding to the 100, 002 and 102 reflections of HCP Y also appear. The ratio of the 101 peak integrated intensities calculated for annealed ribbons to those for fully crystallized ribbons gives an estimate of the rate of Y crystallization. The reaction rates are given in table 1 for ribbons annealed at 533 K as a function of annealing time, together with the Y microcrystal sizes calculated from the width of the 101 reflection using Scherrer's equation for particle size broadening. An eventual broadening due to inhomogeneous

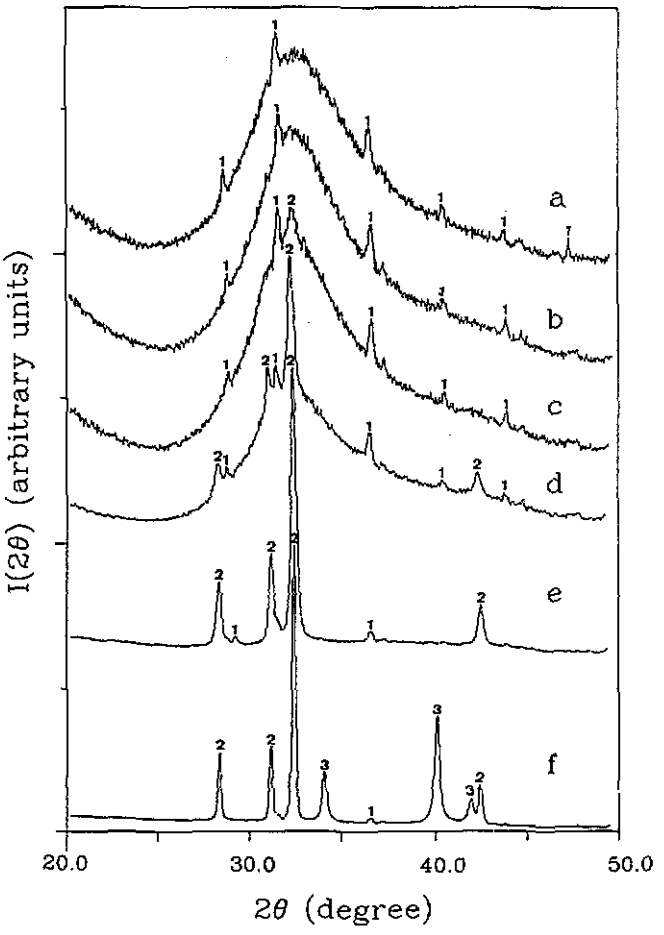

Figure 4. X-ray patterns of $(Fe_{64}Mn_{36})_{35}Y_6$ ribbons using (*a*) as-quenched samples, (*b*)–(*d*) samples annealed at 533 K for (*b*) 3 h, (c) 6 h and (*d*) 24 h, (*e*) partially crystallized samples and (*f*) fully crystallized samples. The numbers 1, 2 and 3 refer to the Y_2O_3 HCP Y and M_2Y laves phases, respectively.

strain cannot be excluded since we are unable to measure it (no series of order of reflections and too small signal-to-background ratios). Nevertheless, the crystallization generally induces only very slight volume changes (here small strains) and so we presume that the particle size broadening is predominant. The comparison of the x-ray patterns in figures 4(*e*) and 4(*f*) shows that the increase in the size of the Y particles starts in particular together with the formation of the Laves phase.

The differential scanning calorimeter measurements have shown changes in the peak temperature T_x of the primary crystallization with annealing treatments. In comparison with as-quenched samples, a small decrease in T_x for ribbons annealed at 533 K for 3 h has been measured which varies from 0.5° to 7.5° when increasing the heating rate α from 20 to 160 K min^{-1}; for $t_a = 6$ h, similar changes have been obtained. For longer times an increase in T_x together with a decrease in the crystallization enthalpy have been observed owing to the onset of Y precipitation during annealing. Using Kissinger's

Table 1. Main parameters for ribbons of $(Fe_{64}Mn_{36})_{35}Y_{65}$ as quenched and annealed at 533 K for different annealing times: reaction rate and diameter D of Y precipitates; correlation length ξ', and limit of the concentration–concentration structure factor $S'_{CC}(0)$ deduced from the OZ plots in the two q-ranges 0.2–0.45 Å^{-1} indicated by superscript 1 and 0.28–0.45 Å^{-1} indicated by superscript 2; ratio of atomic volumes V_M/V_Y determined by the anomalous technique in the q-ranges 0.25–0.45 Å^{-1} (indicated by superscript a) and 0.05–0.15 Å^{-1} (indicated by superscript b).

State of ribbon	Annealing time	Y (%)	D (Å)	ξ^1 (Å)	ξ^2 (Å)	$S^1_{CC}(0)$	$S^2_{CC}(0)$	V^a_M/V_Y	V^b_M/V_Y
As quenched		—	—	7.4	7.2	11.1	10.5	0.32	
Annealed at 533 K	10 min	—	—	7.4	7.4	15.2	15.6	0.39	
Annealed at 533 K	1 h	—	—	6.6	7.3	17	20	0.36	
Annealed at 533 K	6 h	3	≈140	7.2	8.6	20.3	28	0.33	0.33
Annealed at 533 K	24 h	14	≈250	8.9	13	30	59	0.37	0.33
Annealed at 533 K	4 d	28	≈250	11	20	40	125	0.35	0.33

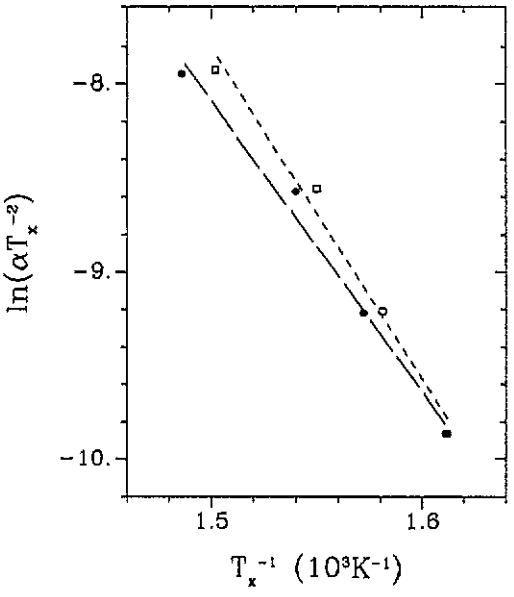

Figure 5. Kissinger plots for $(Fe_{64}Mn_{36})_{35}Y_{65}$ metallic glass using as-quenched samples (●) and samples annealed at 533 K for 3 h (□).

method, the apparent activation energies for the primary crystallization for as-quenched and annealed (533 K, t_a = 3 h) ribbons are determined from the slope of the plots of $\ln(\alpha/T_x^2)$ versus $1/T_x$ (figure 5). The activation energy of 1.55 eV for annealed ribbons is slightly higher than that for as-quenched ribbons which is equal to 1.4 eV, while the crystallization temperature is higher for as-quenched ribbons.

4. Discussion

The absence of an interference halo in the SAXS curves between 0.2 and 0.5 Å^{-1} (figures 1 and 2) indicates that no nanoscopic demixing takes place before the primary crystallization of HCP Y. Consequently, as for as-quenched ribbons (Maret *et al* 1989) the

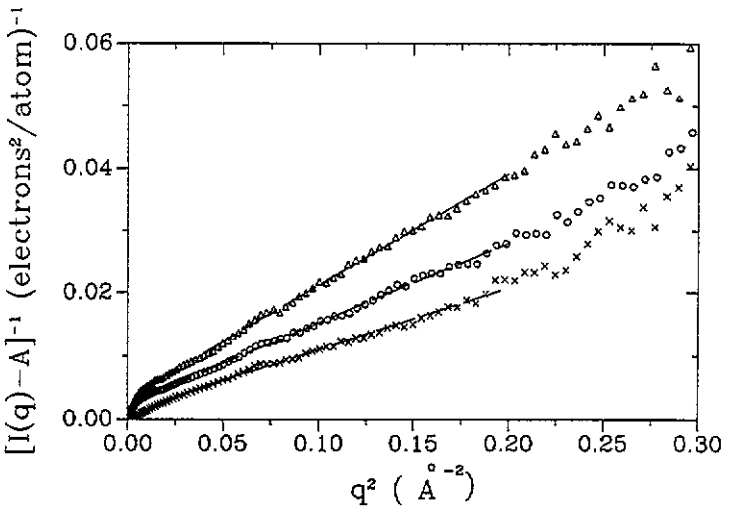

Figure 6. OZ plots for $(Fe_{64}Mn_{36})_{35}Y_{65}$ glass using as-quenched samples (△) and samples annealed at 533 K for 10 mm (○) and 24 h (×).

SAXS curves for annealed ribbons are analysed using the OZ theory and not in a two-phase model. For binary systems, the OZ theory explains the increase in the forward scattering in terms of concentration and density fluctuations, since in the case of a size effect the density fluctuations are related to the concentration fluctuations.

Neglecting all terms of order q^4 and higher, $I(q)$ is described in the small-q region by

$$I(q) = A + B/(1 + \xi^2 q^2). \tag{1}$$

ξ is the correlation length of the concentration fluctuations and B is related to the long-wavelength limit $S_{CC}(0)$ as follows:

$$B = (f_M/V_M - f_Y/V_Y)(f_M/V_M - f_Y/V_Y)^* \times [V_M V_Y/(C_M V_M + C_Y V_Y)]^2 C_M C_Y S_{CC}(0). \tag{2}$$

C_M and C_Y are the atomic concentrations. In equation (1), A is a compressibility term subtracted together with fluorescence and Raman scattering.

The OZ plots for ribbons as quenched and annealed at 533 K for 10 min and 24 h are shown in figure 6; the fits are calculated between 0.2 and 0.45 Å^{-1}. Below 0.2 Å^{-1}, the experimental points deviate from the OZ law, more especially as the annealing time is long owing to the strong scattering of Y precipitates. For samples annealed at 533 K, the values of ξ and $S_{CC}(0)$ deduced from equations (1) and (2) are displayed in figure 7 versus annealing time. In table 1, we give two series of values for ξ and $S_{CC}(0)$ calculated in the q-ranges 0.2–0.45 Å^{-1} and 0.28–0.45 Å^{-1}. The large differences obtained for ribbons annealed for 24 h and 4 d indicate that the values of ξ and $S_{CC}(0)$ are inaccurate (illustrated in figure 7 by large error bars).

In figure 7, we observe an increase in $S_{CC}(0)$ with increasing annealing time which becomes faster for $t_a > 6$ h associated with the onset of crystallization of Y (shown in figure 4 with the appearance of the 101 reflection of HCP Y in the x-ray pattern). The decrease in ξ after a short annealing time seems to be significant since it was already

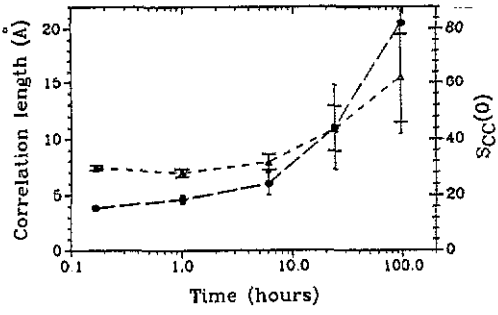

Figure 7. Variation in the correlation length ξ (Δ) and the concentration fluctuations $S_{CC}(0)$ (●) with annealing time at 533 K for $(Fe_{64}Mn_{36})_{35}Y_{65}$ glass.

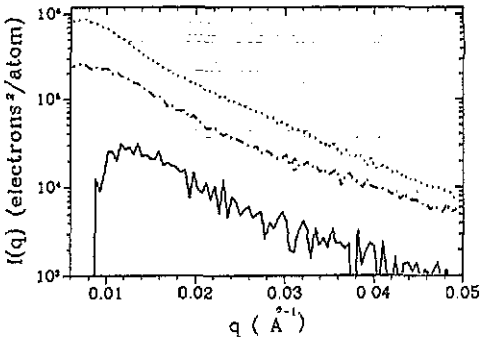

Figure 8. SAXS intensities obtained using a long geometry for $(Fe_{64}Mn_{36})_{35}Y_{65}$ amorphous ribbons which had been annealed at 553 K for 1 h (——), at 533 K for 4 d (— · —) and at 573 K for 30 min (· · · ·) (see also text).

found for ribbons annealed at lower temperatures (Maret *et al* 1989). A minimum value is obtained roughly after an annealing time of 3 h. For $t_a > 3$ h, ξ increases with increasing precipitation of Y. The small decrease in ξ would explain the surprising result of an increase in the activation energy ΔE for ribbons annealed at 533 K for 3 h. ΔE reflects the activation energy not only of growth but also of nucleation. From the classic Becker–Volmer nucleation theory (Fine 1964), the activation energy for nucleation depends on the energy required to form a nucleus of critical size r_c; $r_c = 2\sigma/\Delta G$, where σ is the interfacial energy and ΔG the free-energy difference between the nucleating crystal and the amorphous matrix. The structural relaxation occurring during short-time annealing treatment yields a more stable glass; the driving force for crystallization ΔG is then reduced and, on the assumption that σ does not vary with annealing, the critical radius is larger. Consequently, the size of the regions enriched in Y atoms (given roughly by ξ) deviates more from the size of the critical nucleus for ribbons annealed for a short time than for as-quenched ribbons (r_c being of the order of 10 Å in glasses; see for example the review paper of Scott (1983)). Consequently the nucleation would be more difficult in annealed ribbons associated with a larger activation energy.

Complementary SAXS measurements have been performed using a long geometry with a sample-to-detector distance of 880 mm, which allows one to measure $I(q)$ at smaller scattering vectors ranging from 4×10^{-3} to 5×10^{-2} Å^{-1}. In this q-range, a maximum in the SAXS curves (figure 8) starts to become visible for ribbons containing a percentage of Y particles larger than 5%. To emphasize this effect in the curves shown in figure 8, the contribution of the medium-range order due to concentration fluctuations has been roughly removed by subtracting the intensity measured for a ribbon annealed at 533 K for 1 h. The maximum is attributed to interference effects between Y particles. In spite of the fact that the interference peak is located very close to the transmitted beam, a shift of its position towards smaller q-values from 1.2×10^{-2} to 6×10^{-3} Å^{-1} is still observed when the volume fraction of Y increases. Guinier fits applied beyond this maximum yield particle radii of gyration between 100 and 150 Å.

In summary, the medium-range order already present in the as-quenched ribbons does not entail an amorphous nanophase separation (spinodal like) followed by a polymorphic crystallization of Y (i.e. a nanocrystalline state). Using a long geometry,

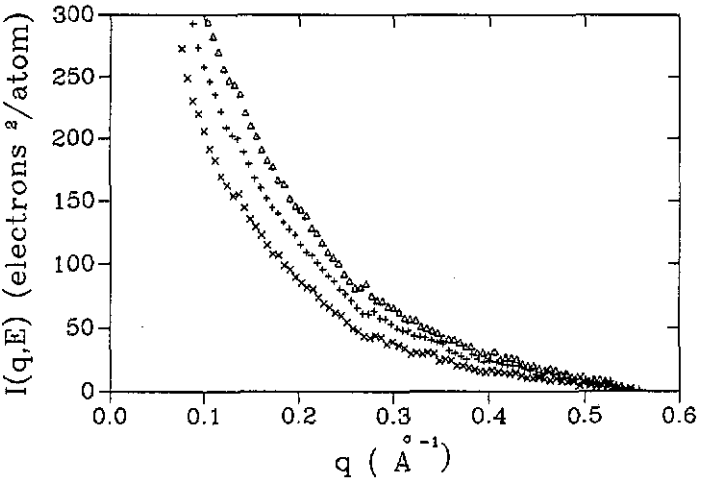

Figure 9. Change in the SAXS intensity with photon energy near the Mn K absorption edge (6539 eV) for ribbons of $(Fe_{64}Mn_{36})_{35}Y_{65}$ annealed at 533 K for 10 min: △, 6261 eV; +, 6490 eV; ×, 6531 eV.

the interference halo produced by the Y precipitates is in part hidden by the beam stop and we especially observe a strong increase in the intensity at small q-vectors superimposed on the signal of the concentration fluctuations. At the end of the primary crystallization of Y, the medium-range order has completely disappeared (see in figure 2 the curve for specimen annealed at 700 K). Consequently, at the onset of crystallization of Y, the increase in the concentration fluctuations and their correlation length together with the volume fraction of Y precipitates indicates that the nucleation of Y stems from the large concentration fluctuations. The nucleation and growth of Y can be classified as a primary crystallization process.

5. Determination of the ratio of the partial atomic volumes by the anomalous small-angle x-ray scattering technique

The SAXS intensities have been measured at three different photon energies: 6261, 6490 and 6531 eV. As illustrated in figure 9, for annealed ribbons, the intensity increases when moving away from the K edge of Mn (6539 eV). Since the absorption coefficient given by $f_i''(E)$ is small compared with $Z_i + f_i'(E)$, $I(q, E)$ corrected for the q-independent contribution can be rewritten from equations (1) and (2) as follows:

$$I(q, E) = [F_M(E)/V_M - F_Y/V_Y]^2 f(q) \tag{3}$$

where $f(q)$, proportional to $S_{CC}(q)$, is a function independent of the photon energy E and $F_M(E)$, the modulus of the complex scattering factor, varies rapidly with E near the K edge of Mn while F_Y remains constant. From equation (3), $\sqrt{I(q, E)}$ and $F_M(E)$ are then linearly correlated and V_M/V_Y is deduced from the slope of the line. In order to increase the precision of V_M/V_Y, $I(q, E)$ is summed over the q-interval 0.25–0.45 Å^{-1} in which the SAXS signal is in great part due to concentration fluctuations, and V_M/V_Y is finally determined from a linear correlation between $\sqrt{\Sigma_q I(q, E)}$ and $F_M(E)$ (see also

Lyon and Simon (1986)). The values denoted V_M^a/V_Y in table 1 for annealed ribbons are always larger than those for as-quenched ribbons and become nearer to the ratio of the atomic volumes of pure components ($V_M^0/V_Y^0 = 0.36$). Looking more carefully, the strongest increase in V_M^a/V_Y is obtained for ribbons annealed at 533 K for relatively short periods. This result can be correlated to the decrease in the correlation length ξ representative of the size of the Y-enriched regions observed after similar annealing times (see figure 7). For long-time annealing, the dispersion of values is attributed to the low level of scattering intensity. For these ribbons, it is more judicious to calculate the ratio V_M/V_Y in an interval at smaller q-values (0.05–0.15 $Å^{-1}$) in which the scattering of Y particles prevails and yields a high level of intensity. The corresponding values, denoted V_M^b/V_Y in table 1, are all equal to 0.33, slightly smaller than the average value of 0.35 found in the other interval.

References

Fine M E 1964 *Phase Transformation in Condensed Systems* (New York: Macmillan)
Lyon O and Simon J P 1986 *Acta Metall.* **34** 1197
Maret M, Simon J P and Lyon O 1989 *J. Phys.: Condens. Matter* **1** 10 249
Scott M G 1983 *Amorphous Metallic Alloys* ed F E Luborsky (London: Butterworths) p 144
Simon J P and Lyon O 1989 *Acta Metall.* **37** 1727